

Deep learning-based breast cancer grading and survival analysis on whole-slide histopathology images

Citation for published version (APA):

Wetstein, S. C., de Jong, V. M. T., Stathonikos, N., Opdam, M., Dackus, G. M. H. E., Pluim, J. P. W., van Diest, P. J., & Veta, M. (2022). Deep learning-based breast cancer grading and survival analysis on whole-slide histopathology images. *Scientific Reports*, 12, Article 15102. <https://doi.org/10.1038/s41598-022-19112-9>

Document license:

CC BY

DOI:

[10.1038/s41598-022-19112-9](https://doi.org/10.1038/s41598-022-19112-9)

Document status and date:

Published: 06/09/2022

Document Version:

Publisher's PDF, also known as Version of Record (includes final page, issue and volume numbers)

Please check the document version of this publication:

- A submitted manuscript is the version of the article upon submission and before peer-review. There can be important differences between the submitted version and the official published version of record. People interested in the research are advised to contact the author for the final version of the publication, or visit the DOI to the publisher's website.
- The final author version and the galley proof are versions of the publication after peer review.
- The final published version features the final layout of the paper including the volume, issue and page numbers.

[Link to publication](#)

General rights

Copyright and moral rights for the publications made accessible in the public portal are retained by the authors and/or other copyright owners and it is a condition of accessing publications that users recognise and abide by the legal requirements associated with these rights.

- Users may download and print one copy of any publication from the public portal for the purpose of private study or research.
- You may not further distribute the material or use it for any profit-making activity or commercial gain
- You may freely distribute the URL identifying the publication in the public portal.

If the publication is distributed under the terms of Article 25fa of the Dutch Copyright Act, indicated by the "Taverne" license above, please follow below link for the End User Agreement:

www.tue.nl/taverne

Take down policy

If you believe that this document breaches copyright please contact us at:

openaccess@tue.nl

providing details and we will investigate your claim.



OPEN

Deep learning-based breast cancer grading and survival analysis on whole-slide histopathology images

Suzanne C. Wetstein¹, Vincent M. T. de Jong², Nikolas Stathonikos³, Mark Opdam², Gwen M. H. E. Dackus^{2,3}, Josien P. W. Pluim¹, Paul J. van Diest³ & Mitko Veta¹✉

Breast cancer tumor grade is strongly associated with patient survival. In current clinical practice, pathologists assign tumor grade after visual analysis of tissue specimens. However, different studies show significant inter-observer variation in breast cancer grading. Computer-based breast cancer grading methods have been proposed but only work on specifically selected tissue areas and/or require labor-intensive annotations to be applied to new datasets. In this study, we trained and evaluated a deep learning-based breast cancer grading model that works on whole-slide histopathology images. The model was developed using whole-slide images from 706 young (< 40 years) invasive breast cancer patients with corresponding tumor grade (low/intermediate vs. high), and its constituents nuclear grade, tubule formation and mitotic rate. The performance of the model was evaluated using Cohen's kappa on an independent test set of 686 patients using annotations by expert pathologists as ground truth. The predicted low/intermediate ($n = 327$) and high ($n = 359$) grade groups were used to perform survival analysis. The deep learning system distinguished low/intermediate versus high tumor grade with a Cohen's Kappa of 0.59 (80% accuracy) compared to expert pathologists. In subsequent survival analysis the two groups predicted by the system were found to have a significantly different overall survival (OS) and disease/recurrence-free survival (DRFS/RFS) ($p < 0.05$). Univariate Cox hazard regression analysis showed statistically significant hazard ratios ($p < 0.05$). After adjusting for clinicopathologic features and stratifying for molecular subtype the hazard ratios showed a trend but lost statistical significance for all endpoints. In conclusion, we developed a deep learning-based model for automated grading of breast cancer on whole-slide images. The model distinguishes between low/intermediate and high grade tumors and finds a trend in the survival of the two predicted groups.

Breast cancer remains one of the leading causes of death in women¹. Most breast cancers are invasive ductal carcinomas of no special type (NST), which arise from epithelial cells lining the ducts. In young patients breast cancers tend to be more aggressive and are considered prognostically unfavorable^{2,3}. As a result, many breast cancer guidelines recommend (neo)adjuvant systemic treatment for nearly all young patients. However, in some patients locoregional treatment alone could be sufficient and systemic therapy would be overtreatment. Overtreatment can cause serious (age-related) side effects, which could have been prevented and therefore accurate prognostication is necessary to reduce the number of overtreatments³.

Histologic tumor grade of NST breast carcinomas is strongly associated with survivorship^{4,5}, also in young breast cancer patients^{6,7}, and is therefore of great importance in clinical prognostics. In current clinical practice, visual assessment of tissue specimens, using hematoxylin and eosin (H&E) stained slides, is the standard practice for determination of, amongst others, histologic grade. This assessment can be done either under a microscope or on digitized whole-slide images (WSI). The grading system widely used is the Nottingham modification of the Bloom-Richardson system^{5,8} which assesses nuclear atypia, mitotic rate, and degree of tubule formation. Pathologists require extensive training and experience to make these visual assessments. Lack of precision in assessing any of the components leads to subjective grading and poor reproducibility among pathologists^{9,10}.

¹Medical Image Analysis Group, Department of Biomedical Engineering, Eindhoven University of Technology, Groene Loper 5, 5612 AE Eindhoven, The Netherlands. ²Department of Molecular Pathology, Netherlands Cancer Institute, Plesmanlaan 121, 1066 CX Amsterdam, The Netherlands. ³Department of Pathology, University Medical Center Utrecht, University Utrecht, Utrecht, The Netherlands. ✉email: m.veta@tue.nl

Automated grading may provide a solution by both decreasing pathologist workload and standardizing clinical practice^{11,12}. Automated methods to process H&E stained breast histopathology images and identify features associated with grading and survival have been developed before. Most early methods focused on hand-crafted or computer extracted features, such as textural and morphological features derived from statistics of shapes^{13–17}. Newer studies that focus on grading and survival prediction by using histopathology images often make use of deep learning^{12,18–23}. Deep learning models have been successfully developed for other tasks in breast histopathology^{24–33}. In breast cancer grading specifically, most early methods focused on predicting the grading components separately. Methods to capture nuclear atypia^{34–38}, tubule formation^{15,39,40} and mitotic count^{28,41} often used labor-intensive nuclei and mitoses annotations as ground truth. These required annotations make it difficult to re-train these methods on newly acquired datasets. More recently, computational pathology methods that work with weak labels on WSI have been developed^{42–46}. Through a principle called multiple instance learning (MIL) it is now possible to train an algorithm on an entire WSI with only a global label (e.g. tumor grade).

In this study, we develop a deep learning-based model for automated grading of NST breast cancer on whole-slide images. The model does not require any labor-intensive annotations and distinguishes between low/intermediate and high grade tumors. Training ($n = 706$) and evaluation ($n = 686$) of this model was done on a large dataset ($n = 1392$ patients) derived from the PARADIGM study² with young (age < 40 years) breast cancer patients. Overall survival (OS), distant recurrence free survival (DRFS) and recurrence free survival (RFS) were compared between the predicted low/intermediate and high tumor grade groups.

Materials and methods

Patient selection and image acquisition. We use data from the PARADIGM study². This study contains all young (age < 40 years) breast cancer patients without (lymph node) metastases, who had no prior malignancy, did not receive adjuvant systemic treatment according to standard practice at the time of diagnosis, and were diagnosed between 1989 and 2000 in The Netherlands ($n = 2286$). The patients were identified through the Netherlands Cancer Registry. Tumor and normal formalin-fixed paraffin-embedded (FFPE) blocks with corresponding pathology reports were retrieved in collaboration with PALGA: Dutch Pathology Registry⁴⁷. For all patients fresh tumor slides were cut and stained with hematoxylin and eosin (H&E). Estrogen receptor, progesterone receptor, and HER2 were evaluated on fresh stained material². We selected all patients diagnosed with pure ‘invasive ductal carcinoma’ (no special type). Furthermore, we selected patients with complete information on hormone receptor status (estrogen receptor and progesterone receptor), HER2 status, tumor grade, and outcome. For each patient, a pathologist selected one representative H&E WSI. The slides were scanned by the Philips UFS scanner 1.6.1.3 RA (Philips, Amsterdam, The Netherlands) or Nanozoomer XR C12000-21/-22 (Hamamatsu photonics, Hamamatsu, Shizuoka, Japan) at 40× magnification with a resolution of 0.22 μm per pixel. Slides scanned with the Philips scanner were converted to JPEG compressed tiff files. We randomly divided patients into a development set and an independent test set. The model was developed at Eindhoven University of Technology while the clinical information of the test set was stored at the Netherlands Cancer Institute, insuring full independence between training and testing datasets. All experiments presented in this paper were performed in accordance with relevant guidelines and regulations (see also “[Ethics approval and consent to participate](#)” section).

Histopathological assessment. Histologic grading of the WSI into grade 1, 2 or 3 was performed according to the “Nottingham modification of the Bloom-Richardson system”^{5,8}. This classification system involves a semi-quantitative evaluation of three morphological components: the degree of nuclear pleomorphism, the percentage of tubular formation and the mitotic count in a defined area. Each component is ascribed a score of 1 to 3 and the final tumor grade is derived from a summation of the three individual components, with grade 1 (low grade) for scores 3–5, grade 2 (intermediate grade) for scores 6–7, and grade 3 (high grade) for scores 8–9.

Tumors were graded by a single pathologist from a team of 16 specialized European breast pathologists each providing the three component grades and the final tumor grade. All grades were converted to low/intermediate (grades 1 and 2) and high grade (grade 3).

Development of the deep learning model. For the development of the deep learning model the patients in the development dataset were randomly assigned to two distinct subsets: training and validation (used for model selection and parameter tuning) datasets. This was separate from our independent test dataset. An overview of the deep learning model and training procedure is presented in Fig. 1.

Pre-processing. WSI are generally too large to use as input for a deep learning model, as a result the images needed to be divided into tiles. In order to extract only tiles containing tissue from the WSI we filtered out tiles with mostly white pixels. All tiles were 224 × 224 pixels and sampled at a 10× magnification level. At this resolution both single nuclei as well as larger structures can be observed.

Multiple instance learning. A WSI can be seen as a “bag” of tiles and the bag label (i.e. the binary tumor grade) is determined by the prevalence of positive (high grade) instances. This means that a bag is classified as positive (high grade) when it contains at least one positive instance and is classified as negative (low/intermediate grade) when all of the tiles are negative. This assumption is called multiple instance learning (MIL) and is the basis of our model.

The deep learning model was based on the MIL model by Campanella et al.⁴². The backbone of the model has a ResNet-34 architecture⁴⁸ which is pre-trained on ImageNet⁴⁹. In the first step, the inference step, 512 randomly selected tissue tiles per WSI were passed through the network to obtain the probability of being high

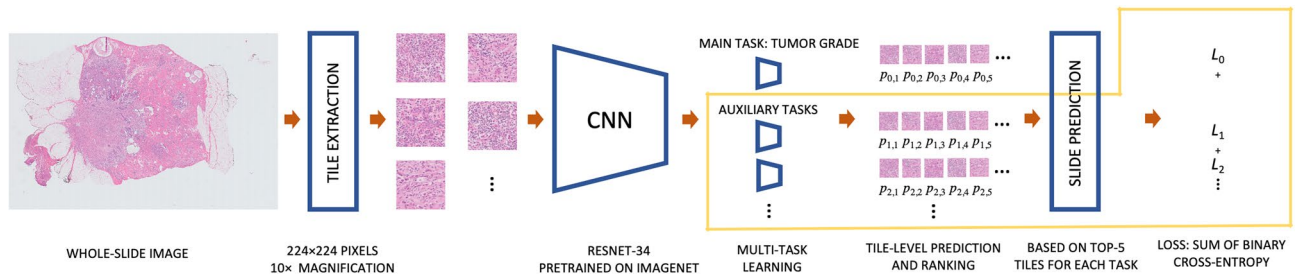


Figure 1. Overview of the deep learning model and training procedure. The components of the model outlined in yellow are used only at training time, this includes the multi-task learning with the auxiliary tasks and the computation of the loss term.

grade for each tile. For each WSI, the top 5 tiles with the highest probability of being high grade were selected. In the second step, these 5 tiles per WSI were used to train the network. Each of these 5 tiles is assigned the same label as the WSI it belongs to. After the training step, the updated model was used for the next iteration of the inference step. At inference time, prediction for the whole-slide image is made by majority voting for the predictions of the top 5 tiles.

Training was done using stochastic gradient descent optimization with a learning rate of 0.007 and a momentum of 0.9. The mini-batch size was 256 and we applied binary cross-entropy loss. For regularization and model robustness, we used a weight decay of 0.01 and data augmentation was applied to each tile. Data augmentation also helped to overcome the variability of the tissue staining appearance, which is an important hurdle in histopathology image analysis⁵⁰. We used a random combination of 90 degree rotations, horizontal and vertical flips, brightness (up to 0.35), contrast (up to 0.5), hue (up to 0.1) and saturation (up to 0.1). The best performing model (based on Cohen's Kappa between predicted and actual tumor grade) after 300 iterations was saved.

Multi-task learning. In this study, we compared a model trained on tumor grade alone with a multi-task learning (MTL) approach in which we trained models to simultaneously predict tumor grade and other prognostic factors. We trained three deep learning models with different target sets and compared them on our internal validation set before applying the best model to the independent test set. The first deep learning model was trained on tumor grade only, the second model was trained on tumor grade and all three component grades and the third model was trained on tumor grade, component grades and hormone receptor and HER2 status. This was done as we believe that adding component grades and hormone receptor and HER2 status can feed extra discriminatory information to the model. It has been shown that auxiliary tasks can improve generalization as an inductive bias is invoked towards representations that also explain these tasks⁵¹.

The inference step was similar for each model as the top 5 tiles were selected based only on tumor grade. The model was extended using a hard parameter sharing approach, meaning that all layers were shared for all targets, except for a final densely connected layer that was specific to each task. The unweighted sum of binary cross-entropy losses of all tasks was used as the loss function.

Statistical analysis. Differences in distributions between the patient characteristics in the development and test dataset were assessed using the Kolmogorov–Smirnov test for continuous variables and Pearson's chi-squared test with Yates' continuity correction for categorical variables.

Agreement in grading between pathologists and our model was measured using Cohen's Kappa and accuracy. Cohen's Kappa is commonly used for inter-rater agreement and ranges from -1 to 1 , with 1 indicating perfect correlation.

Overall survival was defined as the time from diagnosis until death from any cause. Patients were censored if they were alive at eight years of follow-up. Patients that were lost to follow-up were also censored ($n = 6$). Distant recurrence-free survival was defined as the time from diagnosis until a distant recurrence or death from any cause. Patients who had a second primary tumor before distant recurrence were censored at time of second primary ($n = 52$). Recurrence-free survival was defined as the time from diagnosis until a disease recurrence (local, regional, or distant). Patients who had a second primary tumor before recurrence were censored at time of second primary ($n = 48$). Kaplan–Meier survival analysis was performed using log-rank testing. Hazard ratios were obtained using both univariate and multivariate Cox proportional hazards regression. The multivariate regression was adjusted for tumor size, lymphovascular invasion and locoregional treatment. The proportional hazard assumption was tested using schoenfeld residuals. After stratifying the model for molecular subtype (hormone receptor and HER2 status) none of the variables violated the assumption. All deep learning models were trained using Python version 3.6 and implemented using the PyTorch deep learning framework. All survival analyses were performed using R 4.0 (R Core Team, Vienna, Austria), a two-sided $p < 0.05$ was considered statistically significant.

Ethics approval and consent to participate. The PARADIGM initiative will use observational data from the NCR and left over archival patient material. All data and material on the young breast cancer patients involved in this study will be used in a coded way. Neither interventions nor active recruitment of study participants will take place within PARADIGM. As a result, the Dutch law on Research Involving Human Subjects Act

Patient characteristics	Development dataset	Test dataset	<i>p</i> value
<i>n</i>	706	686	
Age at biopsy			1.00
Median years (Interquartile range)	36 (33–38)	36 (33–38)	
Tumor grade (n (%))			0.25
Grade 1	113 (16)	89 (13)	
Grade 2	244 (35)	238 (35)	
Grade 3	349 (49)	359 (52)	
Nuclear score (n (%))			0.66
1	20 (3)	16 (2)	
2	335 (47)	315 (46)	
3	349 (49)	354 (52)	
Tubular score (n (%))			0.62
1	46 (7)	43 (6)	
2	135 (19)	118 (17)	
3	524 (74)	524 (76)	
Mitoses score (n (%))			0.64
1	249 (35)	230 (34)	
2	170 (24)	161 (23)	
3	286 (41)	295 (43)	
Subtype (n (%))			0.06
HR+/HER2–	394 (56)	345 (50)	
HR–/HER2–	182 (26)	218 (32)	
HR+/HER2+	85 (12)	74 (11)	
HR–/HER2+	36 (5)	42 (6)	
Tumor size (n (%))			0.22
1A–B	128 (18)	114 (17)	
1C	365 (52)	366 (54)	
2–3	195 (28)	198 (29)	
Missing	18 (3)	8 (1)	
Lymphovascular invasion (n (%))			0.81
Absent	587 (83)	566 (83)	
Present	119 (17)	120 (17)	
Local treatment (n (%))			0.33
Conserving surgery with radiotherapy	448 (63)	451 (66)	
Mastectomy without radiotherapy	213 (30)	184 (27)	
Other	45 (6)	51 (7)	

Table 1. Patient characteristics of all 1392 women included in our cohort divided in the development dataset ($n = 706$) and test dataset ($n = 686$). *HR* hormone receptor.

(WMO) is not applicable. Therefore, the PARADIGM study received a ‘non-WMO’ declaration from the Medical Ethics Committee of the Netherlands Cancer Institute—Antoni van Leeuwenhoek hospital (NKI), waiving individual patient consent, on 31 October 2012 (PTC 12.1489/NBCP project). In addition, approval from the NKI translational research board (TRB) was obtained.

Results

Population characteristics. Patient characteristics for our development ($n = 706$) and test ($n = 686$) dataset are summarized in Table 1. The median age for patients in both development and test datasets was 36 years. The distribution of tumor grade and component grades in low/intermediate (grade 1 and 2) versus high grade (grade 3) tumors between the development and test dataset varied by less than 3%. The grade distribution for WSI scanned by the two scanners used in this study were similar (Supplementary Information Table S1). The most common tumor subtype in our dataset was hormone receptor +/HER2–, 56% versus 50% in the development and test dataset respectively. No significant differences were found in the distribution of characteristics between the development and test dataset.

Model selection on the validation set. Agreement between pathologist and three deep learning models on NST tumor grading is shown in Table 2. The deep learning model trained on tumor grade alone achieved a Cohen’s Kappa score of 0.54 compared to pathologists. The model trained on tumor grade and the three grade com-

Model targets	Cohen's Kappa (SD)	Accuracy (SD)
Tumor grade only	0.54 (± 0.10)	0.77 (± 0.05)
Tumor grade and component grades	0.61 (± 0.09)	0.80 (± 0.05)
Tumor grade, component grades and HR and HER2 status	0.58 (± 0.09)	0.79 (± 0.05)

Table 2. Agreement and accuracy of model versus pathologist grading of no special type (NST) tumors. The results for three models trained on different sets of targets are shown on the validation set ($n = 142$). The standard deviation (SD) was calculated using bootstrapping. *HR* hormone receptor.

Target	Cohen's Kappa (SD)	Accuracy (SD)
Tumor grade	0.59 (± 0.04)	0.80 (± 0.02)
Nuclear score	0.41 (± 0.04)	0.70 (± 0.02)
Tubular score	0.35 (± 0.04)	0.70 (± 0.02)
Mitoses score	0.53 (± 0.04)	0.77 (± 0.02)

Table 3. Agreement and accuracy of model versus pathologists grading, overall as well as split by nuclear pleomorphism, tubular differentiation and mitotic count. Results are shown on the test set ($n = 686$). The standard deviation (SD) was calculated using bootstrapping.

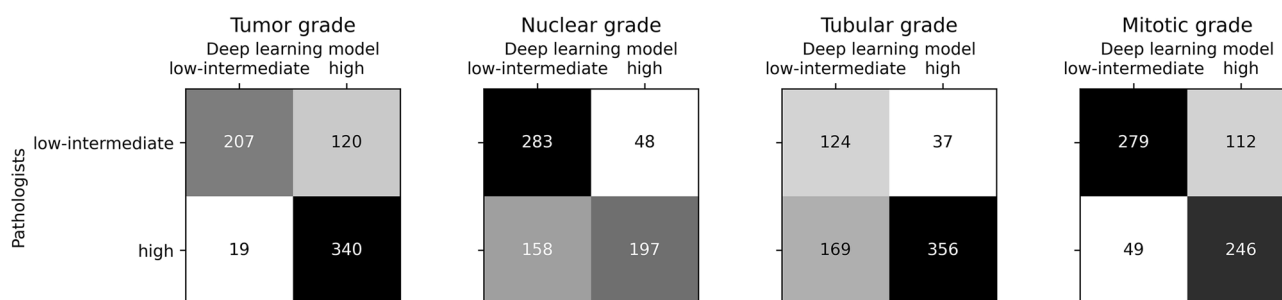


Figure 2. Confusion matrices for no special type (NST) tumor grading and grade components (nuclear, tubular and mitoses scores) between pathologists and the deep learning model. These results are on the test set ($n = 686$).

ponents achieved a Cohen's Kappa score of 0.61 and the model trained on tumor grade, grade components and hormone receptor and HER2 status achieved a Cohen's Kappa score of 0.58. Although the three models performed comparably, we decided to select the model trained on tumor grade and the three grade components to be applied to the test set. We selected this model as it achieved the highest Kappa score and adding the three grading components to the model adds information that pathologists also use when grading. Further results in this paper are based on this model only.

Final model results on the test set. *Tumor grading.* Deep learning model versus pathologist agreement for tumor grading and the three grade components is shown in Table 3. Agreement on overall tumor grade between the deep learning model and pathologists was 0.59. The confusion matrices of inter-observer agreement on tumor grading and the grade components can be found in Fig. 2. Interestingly, nuclear and tubular scores showed high numbers of false negatives (23% and 25%), while mitoses score and tumor grading itself showed higher numbers of false positives (16% and 17%).

Our model predicts the probability of a tile being high grade cancer for each tile in the WSI. With this information we have created tile-based heatmaps overlaid on the WSI. These heatmaps and the 5 tiles with the highest probability of being high grade are shown in Fig. S1 of the Supplementary Information for 8 WSI.

Survival analysis. Kaplan–Meier curves for patients grouped by low/intermediate versus high grade are shown in Fig. 3. For both pathologists and the deep learning model high grade tumors had a worse prognosis compared to low/intermediate grade tumors for all survival endpoints (OS, DRFS, and RFS). The 8-year survival rates of the low/intermediate and high grade groups as assigned by pathologists and the deep learning model for all survival endpoints are shown in Table 4.

We further performed univariable and multivariable Cox regressions for both the deep learning model and pathologist grading. Results of the univariable analysis are shown in Table 5. We found that the deep learning model and pathologist-assigned low/intermediate versus high grade groups were significantly associated with all endpoints ($p < 0.05$). In the multivariable Cox regression, stratified for molecular subtype, the pathologist groups

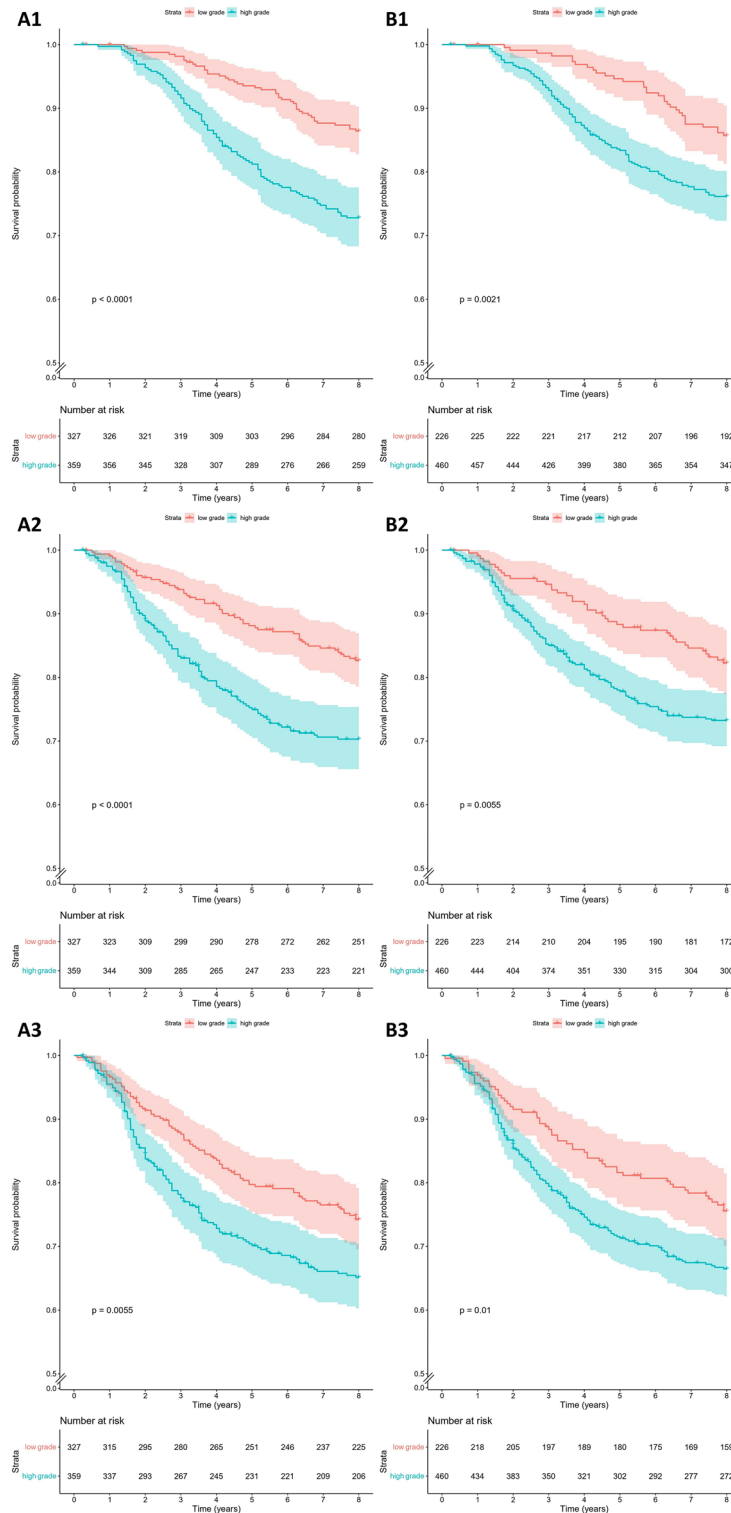


Figure 3. Kaplan–Meier survival curves for young breast cancer patients grouped by low/intermediate versus high grade tumors as assigned by pathologists (A) and the deep learning model (B) for overall survival (1), distant recurrence free survival (2) and recurrence free survival (3). These results are on the test set ($n = 686$).

were still significantly associated with OS and DRFS ($p < 0.05$). The deep learning model, however, showed a trend but lost statistical significance (Table 6). Both the pathologist- and model-defined groups were not significantly associated with RFS after adjustment for clinicopathologic features.

Survival endpoint	8-year survival rate (% (95% CI))	
	Pathologists	Deep learning model
OS		
Low/intermediate grade	85.7 (81.3–90.4)	86.4 (82.8–90.2)
High grade	76.1 (72.3–80.2)	72.8 (68.3–77.6)
DRFS		
Low/intermediate grade	82.7 (78.6–86.9)	82.3 (77.4–87.5)
High grade	70.3 (65.6–75.4)	73.2 (69.2–77.5)
RFS		
Low/intermediate grade	74.2 (69.6–79.2)	75.6 (70.1–81.5)
High grade	65.1 (60.3–70.4)	66.5 (62.2–71.1)

Table 4. Eight-year survival rates of low/intermediate and high grade groups as assigned by pathologists and the deep learning model for overall survival (OS), distant recurrence free survival (DRFS) and recurrence free survival (RFS). Results are shown on the test set ($n = 686$).

Survival endpoint	Pathologists		Deep learning model	
	Hazard ratio (95% CI)	<i>p</i> value	Hazard ratio (95% CI)	<i>p</i> value
Overall survival	2.23 (1.56–3.19)	<0.001	1.84 (1.24–2.72)	0.025
Distant recurrence free survival	1.92 (1.38–2.67)	<0.001	1.66 (1.16–2.39)	0.006
Recurrence free survival	1.49 (1.12–1.97)	0.006	1.50 (1.10–2.05)	0.011

Table 5. Univariate hazard ratios showing the prognostic value of high versus low/intermediate grade tumors as assessed by pathologists or the deep learning model for different survival endpoints. Results are shown on the test set ($n = 686$).

Discussion

In this study, we trained a deep learning-based breast cancer grading model that works on entire WSI. The model distinguishes between low/intermediate and high grade tumors and also predicts nuclear, mitotic and tubular grade. It was developed using a dataset of H&E WSI from young breast cancer patients, a group for whom current breast cancer prognostication tools are not adequately validated². The deep learning-based breast cancer grading model was able to pick-up a non-significant trend in outcome between the two predicted grade groups (low/intermediate vs. high).

The inter-observer agreement between the model and pathologists, as measured by Cohen's Kappa, was 0.59 (accuracy 80%) for distinguishing between low/intermediate and high tumor grade on the test set, which is considered moderate. Tumors with pathologist-defined intermediate grade were more likely to be misclassified as high grade tumors by the model than pathologist-defined low grade tumors (results not shown). The agreement of the trained model with the grading of pathologists was slightly lower than the agreement found between two breast pathologists for the same task on a different dataset (kappa 0.78, accuracy 89%)²³.

Using our model we also evaluated grading components separately (nuclear, tubular, and mitosis scores). We found Kappa scores for model versus pathologist agreement between low/intermediate and high grade of 0.41, 0.35, and 0.53, for the nuclear, tubular, and mitotic component, respectively. In contrast to our results, previous studies among pathologists found scoring tubule formation was more reproducible than scoring either nuclear pleomorphism or mitotic count^{52–55}. We assume, that the low reproducibility of tubular grade in our study is due to the MIL framework not being suited to scoring this component. The model predicts grades for each component based on the top 5 tiles extracted from the WSI that are predicted to have the highest overall tumor grade. Nuclear pleomorphism and mitotic count can easily be scored on these top 5 tiles. However, since tubular formation is scored as a percentage of the entire tumor area, the model prediction based on only 5 tiles seems not to be able to fulfill this task.

Our method is based on the MIL methodology developed by Campanella et al.⁴². The method was originally tested on tasks and datasets that are substantially different than our tasks (prostate, skin and lymph node status) so a direct comparison of the performance is not adequate. We used a version of the method that works with 10× magnification, which offers a good compromise between details of the morphology that are visible and computational speed. We selected this magnification offers a good balance between each tile containing tissue architecture information and sufficient details of the morphology of the individual nuclei.

Since the dataset that we used for developing our model contained additional global labels, such as the different components of the grade and HR and HER2 status we investigated a multi-task learning approach. Such models can learn better (based on multiple tasks) representation of the image data and should always be investigated if such auxiliary tasks are available. The MTL model that in addition to the tumor grade also predicts the grade components resulted in the highest Cohen's kappa and accuracy on the validation set and was used in all subsequent analyses on the test set.

Survival endpoint	Variables	Pathologists		Deep learning model	
		Hazard ratio (95% CI)	p value	Hazard ratio (95% CI)	p value
Overall survival	Tumor grade				
	Low/intermediate	REF		REF	
	High	1.87 (1.24–2.82)	< 0.01	1.39 (0.89–2.18)	0.15
	Tumor size				
	1A–B	REF		REF	
	1C	1.59 (0.91–2.79)	0.11	1.67 (0.95–2.92)	0.07
	2–3	1.54 (0.85–2.80)	0.15	1.67 (0.93–3.03)	0.09
	Lymphovascular invasion				
	Absent	REF		REF	
	Present	2.45 (1.68–3.56)	< 0.01	2.61 (1.80–3.78)	< 0.01
	Local treatment				
	Conserving surgery with radiotherapy	REF		REF	
Mastectomy without radiotherapy	0.96 (0.64–1.44)	0.84	1.02 (0.68–1.52)	0.93	
Other	2.23 (1.29–3.85)	< 0.01	2.30 (1.33–3.98)	< 0.01	
Distant recurrence free survival	Tumor grade				
	Low/intermediate	REF		REF	
	High	1.70 (1.16–2.48)	< 0.01	1.49 (0.99–2.25)	0.06
	Tumor size				
	1A–B	REF		REF	
	1C	2.15 (1.19–3.89)	0.01	2.23 (1.23–4.02)	< 0.01
	2–3	2.57 (1.39–4.75)	< 0.01	2.72 (1.48–5.02)	< 0.01
	Lymphovascular invasion				
	Absent	REF		REF	
	Present	2.70 (1.91–3.82)	< 0.01	2.87 (2.03–4.04)	< 0.01
	Local treatment				
	Conserving surgery with radiotherapy	REF		REF	
Mastectomy without radiotherapy	1.08 (0.75–1.57)	0.67	1.15 (0.79–1.66)	0.47	
Other	2.24 (1.32–3.81)	< 0.01	2.31 (1.36–3.94)	< 0.01	
Recurrence free survival	Tumor grade				
	Low/intermediate	REF		REF	
	High	1.30 (0.94–1.80)	0.12	1.37 (0.96–1.96)	0.08
	Tumor size				
	1A–B	REF		REF	
	1C	1.64 (1.02–2.61)	0.04	1.65 (1.04–2.63)	0.03
	2–3	1.93 (1.18–3.17)	< 0.01	1.97 (1.21–3.21)	< 0.01
	Lymphovascular invasion				
	Absent	REF		REF	
	Present	2.70 (1.98–3.68)	< 0.01	2.75 (2.02–3.73)	< 0.01
	Local treatment				
	Conserving surgery with radiotherapy	REF		REF	
Mastectomy without radiotherapy	1.00 (0.72–1.39)	1.00	1.02 (0.74–1.42)	0.88	
Other	1.72 (1.05–2.82)	0.03	1.74 (1.06–2.85)	0.03	

Table 6. Multivariate hazard ratios showing the prognostic value of high versus low/intermediate grade tumors as assessed by pathologists or the deep learning model for different survival endpoints. This model was stratified by molecular subtype. Results are shown on the test set ($n = 686$).

Despite successfully performing deep learning models for breast histopathology tasks^{23–32}, using deep learning is discouraged due to its lack of interpretability^{56,57}. To better interpret the results of the model we created heatmaps (at the tile level) and extracted the top 5 tiles for 8 WSI shown in Supplementary Information Fig. S1. These heatmaps make it possible for pathologists to see which regions the model considers when making decisions.

Supplementary Information Fig. S1 shows that, although no tumor annotations were used in this study, the model clearly focuses on the tumor area when grading. Furthermore, the top 5 selected tiles for high grade tumors often contain high nuclear scores and high mitotic activity. Such correlations between the morphological appearance of the tissue (such as the size, texture and type of nuclei and their organization) of the selected tiles and the predicted class label of the model should be further investigated in future work with the goal of improved interpretability of the model. Furthermore, if used in clinical practice, interpretability tools can be used by clinicians for rejecting spurious predictions (e.g. if the selected tiles are clearly located in irrelevant areas such as fat tissue). However, the precise mechanism of this should be further investigated in future work.

When assessing potential biomarkers, both robustness and validity are essential to confirm clinical applicability. Deep learning models are robust in the sense that the exact same slide, per definition, will always produce the same grade. However, this may not hold if the slide was scanned on a different scanner or was otherwise changed (e.g. due to faded staining). Our results were validated by analysis on a large ($n = 686$) independent, but similar sample set. This test set included samples from different institutes but all slides were, stained and scanned at the same institute. However, FFPE was made in different institutes.

Kaplan–Meier survival analysis showed a significant difference ($p < 0.05$) in OS, DRFS and RFS for both pathologist- and model-defined low/intermediate versus high grade groups on our test set. In all cases, the difference between the two groups is slightly larger for pathologist-defined groups. Univariable hazard ratios for OS, DRFS and RFS Cox regression were statistically significant for both the model and pathologists ($p < 0.05$). After adjusting for clinicopathologic features and stratifying for molecular subtype the hazard ratios were still significant for pathologists (OS and DRFS) but not for the deep learning-based model, which showed a non-significant trend. Currently pathologists are better at predicting patient outcomes than the deep learning model. However, the trend that the deep learning model shows holds promise for the future.

Our model offers some important advances over previously described breast cancer grading models with comparable performance (e.g.²³). Firstly, the fact that it was developed using a weakly supervised learning approach without time-consuming detailed annotations. This means that the model can be directly applied to a WSI (no specific manual area selection needed). Secondly, our work distinguishes itself because it was developed on a large dataset of WSI from young breast cancer patients. The trained model shows promise for further development and validation of prognostic deep learning-based tools in this group. Thirdly, the model we have trained is interpretable for pathologists because it can show which regions in a WSI it uses for its assessment of tumor grade. This is an important step for the adoption of these models as a second reader in daily clinical practice.

Our work should be viewed in light of some limitations. Firstly, our model only discerns low/intermediate from high grade tumors and cannot discern between low (grade 1) and intermediate (grade 2) tumors. Grade 1 tumors have a more favourable clinical course and this highly relevant clinical information is lost when using the model. Secondly, our analysis lacks several control groups. The first control group would regard WSI scanning. Our study includes two different scanners but each WSI was only scanned by one scanner. Re-scanning slides on both platforms could help us compare robustness and validity of grade estimates. The second control group could be created by having multiple pathologists grade each WSI. Breast cancer grading remains difficult and could result in moderate reproducibility of tumor grade^{10,52}. In this study, the WSI were each graded by a single pathologist from a group of very experienced breast pathologists. Insufficient consistency between tumor grades in the training dataset can make it harder for the model to learn correct patterns for the different grades. To create a model for objective breast cancer grading, objective ground truth annotations need to exist. In this dataset higher quality grades for training and testing could be achieved by using consensus grades of multiple pathologists for each WSI. Thirdly, due to the skewed distribution of breast cancer molecular subtypes in young patients we cannot be sure that the model will perform similarly for older women with breast cancer. Finally, it should be noted that deep learning models are made to function in developed countries with state-of-the-art laboratories that have all needed hardware and software in place. These techniques are, therefore, not available to everyone, everywhere.

Another way to work with more objective targets would be to train our model on survival endpoints directly. Future work can include the investigation of a fully automated approach for breast cancer prognostication. Our model could directly be used to predict binary 5 or 10-year survival on WSI. Furthermore, it could be adapted to work with Cox proportional hazards like several groups working on other pathology tissues have done^{58–60}. Prior work on deep learning for breast cancer prognostication specifically has used existing clinically validated risk models (such as ROR-PT score²³) as a proxy for long term outcome, but none have predicted survival directly.

In conclusion, we have trained a deep learning-based breast cancer grading model. The model can be applied to entire WSI directly, does not need time-consuming detailed annotations and was validated on a large dataset of young breast cancer patients. It distinguishes between low/intermediate and high grade tumors and shows a non-significant trend for the prediction of patient outcome. This model is a first step, and is not yet ready to be applied in clinical practice as at this point in time pathologists still outperform the model in predicting survival. Furthermore, any potential sources of bias in the predictions should be thoroughly investigated before applying such a model in practice. In the future deep learning models may be used to aid pathologists in making even more robust assessment of breast cancer tumor grade, especially in cases with less straight forward morphology. In addition, future work may include the investigation of a fully automated approach for breast cancer prognostication using deep learning-based models like ours to directly predict patient outcome on WSI.

Data availability

Subject clinical data, whole slide images, and pathological reviews that support the findings of this study are not publicly available. The survival data that support the findings of this study are available from the Netherlands Cancer Registry, hosted by the Netherlands Comprehensive Cancer Centre (IKNL) but restrictions apply to

the availability of these data, which were used under license for the current study. Data are available from the authors upon reasonable request and with permission of The Netherlands Comprehensive Cancer Centre (IKNL).

Received: 22 December 2021; Accepted: 24 August 2022

Published online: 06 September 2022

References

- Siegel, R. L., Miller, K. D. & Jemal, A. Cancer statistics, 2020. *CA Cancer J. Clin.* **65**(1), 5–29 (2020).
- Dackus, G. M. *et al.* Long-term prognosis of young breast cancer patients (≤ 40 years) who did not receive adjuvant systemic treatment: Protocol for the PARADIGM initiative cohort study. *BMJ Open* **7**(11), e017842 (2017).
- Anders, C. K., Johnson, R., Litton, J., Phillips, M. & Bleyer, A. Breast cancer before age 40 years. *Semin. Oncol.* **36**(3), 237–249 (2009).
- Dunnwald, L. K. & Rossing, M. A. Li CI (2007) Hormone receptor status, tumor characteristics, and prognosis: A prospective cohort of breast cancer patients. *Breast Cancer Res.* **9**(1), 1–10 (2007).
- Elston, C. W. & Ellis, I. O. Pathological prognostic factors in breast cancer. I. The value of histological grade in breast cancer: Experience from a large study with long-term follow-up. *Histopathology* **19**(5), 403–410 (1991).
- Colak, D. *et al.* Agespecific gene expression signatures for breast tumors and crossspecies conserved potential cancer progression markers in young women. *PLoS ONE* **8**(5), e63204 (2013).
- Sundquist, M., Thorstenson, S., Brudin, L., Wingren, S. & Nordenskjold, B. Incidence and prognosis in early onset breast cancer. *Breast* **11**(1), 30–35 (2002).
- Bloom, H. & Richardson, W. Histological grading and prognosis in breast cancer: A study of 1409 cases of which 359 have been followed for 15 years. *Br. J. Cancer* **11**(3), 359 (1957).
- Tawfik, O. *et al.* Grading invasive ductal carcinoma of the breast: Advantages of using automated proliferation index instead of mitotic count. *Virchows Arch.* **450**(6), 627–636 (2007).
- Van Doijeweert, C. *et al.* Significant inter- and intra-laboratory variation in grading of invasive breast cancer: A nationwide study of 33,043 patients in the Netherlands. *Int. J. Cancer* **146**(3), 769–780 (2020).
- Dimitriou, N., Arandjelović, O. & Caie, P. D. Deep learning for whole slide image analysis: An overview. *Front. Med.* **6**, 264 (2019).
- Litjens, G. *et al.* Deep learning as a tool for increased accuracy and efficiency of histopathological diagnosis. *Sci. Rep.* **6**, 26286 (2016).
- Beck, A. H. *et al.* Systematic analysis of breast cancer morphology uncovers stromal features associated with survival. *Sci. Transl. Med.* **3**(108), 108ra113 (2011).
- Yuan, Y. *et al.* Quantitative image analysis of cellular heterogeneity in breast tumors complements genomic profiling. *Sci. Transl. Med.* **4**(157), 157ra143 (2012).
- Ojansivu, V. *et al.* Automated classification of breast cancer morphology in histopathological images. *Diagn. Pathol.* **8**(1), 1–4 (2013).
- Wan, T., Cao, J., Chen, J. & Qin, Z. Automated grading of breast cancer histopathology using cascaded ensemble with combination of multi-level image features. *Neurocomputing* **229**, 34–44 (2017).
- Dimitropoulos, K. *et al.* Grading of invasive breast carcinoma through Grassmannian VLAD encoding. *PLoS ONE* **12**(9), e0185110 (2017).
- Bulten, W. *et al.* Automated deep-learning system for Gleason grading of prostate cancer using biopsies: A diagnostic study. *Lancet Oncol.* **21**, 233–241 (2020).
- Ertosun, M. G. & Rubin, D. L. Automated grading of gliomas using deep learning in digital pathology images: A modular approach with ensemble of convolutional neural networks. In *AMIA Annual Symposium Proceedings 2015*, 1899–908 (2015).
- Källén, H., Molin, J., Heyden, A., Lundström, C. & Åström, K. Towards grading gleason score using generically trained deep convolutional neural networks. In *Proceedings of the 13th International Symposium on Biomedical Imaging (ISBI) 2016*, 1163–1167 (2016).
- Yue, X., Dimitriou, N., Caie, D. P., Harrison, J. D. & Arandjelovic, O. Colorectal cancer outcome prediction from H&E whole slides images using machine learning and automatically inferred phenotype profiles. In *Conference on Bioinformatics and Computational Biology* Vol. 60, 139–149 (2019).
- Wetstein, S. C. *et al.* Deep learning-based grading of ductal carcinoma in situ in breast histopathology images. *Lab. Invest.* **101**, 525–533 (2021).
- Couture, H. D. *et al.* Image analysis with deep learning to predict breast cancer grade, ER status, histologic subtype, and intrinsic subtype. *NPJ Breast Cancer* **4**(1), 1–8 (2018).
- Veta, M. *et al.* Predicting breast tumor proliferation from whole-slide images: The TUPAC16 challenge. *Med. Image Anal.* **54**, 111–121 (2019).
- Wetstein, S. C. *et al.* Deep learning assessment of breast terminal duct lobular unit involution: Towards automated prediction of breast cancer risk. *PLoS ONE* **15**, e0231653 (2020).
- Kensler, K. H. *et al.* Automated quantitative measures of terminal duct lobular unit involution and breast cancer risk. *Cancer Epidemiol. Biomark. Prev.* **29**, 2358–2368 (2020).
- Bejnordi, B. E. *et al.* Using deep convolutional neural networks to identify and classify tumor-associated stroma in diagnostic breast biopsies. *Mod. Pathol.* **31**, 1502 (2018).
- Balkenhol, M. C. A. *et al.* Deep learning assisted mitotic counting for breast cancer. *Lab. Invest.* **99**, 1596–1606 (2019).
- Veta, M., van Diest, P. J., Jiwa, M., Al-Janabi, S. & Pluim, J. P. W. Mitosis counting in breast cancer: Object-level interobserver agreement and comparison to an automatic method. *PLoS ONE* **11**, e0161286 (2016).
- Wang, D., Khosla, A., Gargeya, R., Irshad, H. & Beck, A. H. Deep learning for identifying metastatic breast cancer. Preprint at <https://arxiv.org/abs/1606.05718> (2016).
- Bejnordi, B. E. *et al.* Diagnostic assessment of deep learning algorithms for detection of lymph node metastases in women with breast cancer. *JAMA* **318**, 2199–2210 (2017).
- Bejnordi, B. E. *et al.* Automated detection of DCIS in whole-slide H&E stained breast histopathology images. *IEEE Trans. Med. Imaging* **35**, 2141–2150 (2016).
- Wang, Y. *et al.* Improved breast cancer histological grading using deep learning. *Ann. Oncol.* **33**, 89–98 (2022).
- Khan, A. M., Sirinukunwattana, K. & Rajpoot, N. A global covariance descriptor for nuclear atypia scoring in breast histopathology images. *IEEE J. Biomed. Health Inform.* **19**(5), 1637–1647 (2015).
- Lu, C., Ji, M., Ma, Z. & Mandal, M. Automated image analysis of nuclear atypia in high-power field histopathological image. *J. Microsc.* **258**(3), 233–240 (2015).
- Rezaeilouyeh, H., Mollahosseini, A. & Mahoor, M. H. Microscopic medical image classification framework via deep learning and shearlet transform. *J. Med. Imaging* **3**(4), 044501 (2016).
- Xu, J., Zhou, C., Lang, B. & Liu, Q. Deep learning for histopathological image analysis: Towards computerized diagnosis on cancers. In *Deep Learning and Convolutional Neural Networks for Medical Image Computing*, 73–95 (2017).

38. Das, A., Nair, M. S. & Peter, S. D. Computer-aided histopathological image analysis techniques for automated nuclear atypia scoring of breast cancer: A review. *J. Digit. Imaging* **33**(5), 1091–1121 (2020).
39. Basavanahally, A. *et al.* Incorporating domain knowledge for tubule detection in breast histopathology using O’Callaghan neighborhoods. In *Medical Imaging 2011: Computer-Aided Diagnosis* Vol. 7963, 796310 (2011).
40. Romo-Bucheli, D., Janowczyk, A., Gilmore, H., Romero, E. & Madabhushi, A. Automated tubule nuclei quantification and correlation with oncotype DX risk categories in ER+ breast cancer whole slide images. *Sci. Rep.* **6**(1), 1–9 (2016).
41. Veta, M. *et al.* Assessment of algorithms for mitosis detection in breast cancer histopathology images. *Med. Image Anal.* **20**(1), 237–248 (2015).
42. Campanella, G. *et al.* Clinical-grade computational pathology using weakly supervised deep learning on whole slide images. *Nat. Med.* **25**(8), 1301–1309 (2019).
43. Lu, M. Y. *et al.* Data-efficient and weakly supervised computational pathology on whole-slide images. *Nat. Biomed. Eng.* **5**(6), 555–570 (2021).
44. Naik, N. *et al.* Deep learning-enabled breast cancer hormonal receptor status determination from base-level H&E stains. *Nat. Commun.* **11**(1), 1–8 (2020).
45. Kanavati, F. *et al.* Weakly-supervised learning for lung carcinoma classification using deep learning. *Sci. Rep.* **10**(1), 1–11 (2020).
46. Bilal, M. *et al.* Novel deep learning algorithm predicts the status of molecular pathways and key mutations in colorectal cancer from routine histology images. Preprint at <https://www.medrxiv.org/content/10.1101/2021.01.19.21250122v2.full> (2021).
47. Casparie, M. *et al.* Pathology databanking and biobanking in The Netherlands, a central role for PALGA, the nationwide histopathology and cytopathology data network and archive. *Anal. Cell Pathol.* **29**(1), 19–24 (2007).
48. He, K., Zhang, X., Ren, S. & Sun, J. Deep residual learning for image recognition. In *Proceedings of IEEE Conference on Computer Vision and Pattern Recognition 2016*, 770–778 (2016).
49. Deng, J. *et al.* Imagenet: A large-scale hierarchical image database. In *Proceedings of IEEE Conference on Computer Vision and Pattern Recognition 2009*, 248–255 (2009).
50. Lafarge, M. W., Pluim, J. P. W., Eppenhof, K. A., Moeskops, P. & Veta, M. Domain-adversarial neural networks to address the appearance variability of histopathology images. In *Deep Learning in Medical Image Analysis and Multimodal Learning for Clinical Decision Support 2017*, 83–91 (2017).
51. Caruana, R. Multitask learning. *Mach. Learn.* **28**(1), 41–75 (1997).
52. Frierson, H. F. Jr. *et al.* Interobserver reproducibility of the Nottingham modification of the Bloom and Richardson histologic grading scheme for infiltrating ductal carcinoma. *Am. J. Clin. Pathol.* **103**(2), 195–198 (1995).
53. Delides, G. S. *et al.* Intralaboratory variations in the grading of breast carcinoma. *Arch. Pathol. Lab. Med.* **106**(3), 126–128 (1982).
54. Theissig, F., Kunze, K. D., Haroske, G. & Meyer, W. Histological grading of breast cancer: Interobserver, reproducibility and prognostic significance. *Pathol. Res. Pract.* **186**(6), 732–736 (1990).
55. Harvey, J. M., de Klerk, N. H. & Sterrett, G. F. Histological grading in breast cancer: Interobserver agreement, and relation to other prognostic factors including ploidy. *Pathology* **24**(2), 63–68 (1992).
56. Holzinger, A., Biemann, C., Pattichis, C. S. & Kell, D. B. What do we need to build explainable AI systems for the medical domain? Preprint at <https://arxiv.org/abs/1712.09923> (2017).
57. Lipton, Z. C. The mythos of model interpretability: In machine learning, the concept of interpretability is both important and slippery. *Queue* **16**(3), 31–57 (2018).
58. Zhu, X., Yao, J., Zhu, F. & Huang, J. Wsisa: Making survival prediction from whole slide histopathological images. In *Proceedings of IEEE Conference on Computer Vision and Pattern Recognition 2017*, 7234–7242 (2017).
59. Mobadersany, P. *et al.* Predicting cancer outcomes from histology and genomics using convolutional networks. *Proc. Natl. Acad. Sci.* **115**(13), E2970–E2979 (2018).
60. Tang, B., Li, A., Li, B. & Wang, M. CapSurv: Capsule network for survival analysis with whole slide pathological images. *IEEE Access* **7**, 26022–26030 (2019).

Acknowledgements

We thank Sabine C. Linn for her part in conceiving and designing the study and for scientific advice. We would like to acknowledge the Core Facility Molecular Pathology & Biobanking (CFMPB) of the Netherlands Cancer Institute for supplying tissue material and lab support. The authors thank the registration team of the Netherlands Comprehensive Cancer Organisation (IKNL) for the collection of data for the Netherlands Cancer Registry as well as IKNL staff for scientific advice. We would like to acknowledge PALGA: Dutch Pathology Registry for data provision.

Author contributions

Conceived and designed the study: M.V., P.J.D., S.C.W., V.J. Collection of PARADIGM data: P.J.D., G.M.H.E.D., M.O., N.S., V.J. Image processing, development and implementation of the automated method: S.C.W., M.V., J.P.W.P., N.S. Data analyses: S.C.W., M.V., V.J. All authors contributed to the writing and reviewing of the manuscript.

Funding

The authors would like to thank The Netherlands Organisation for Health Research and Development (ZonMW) Project number 836021019, A Sisters Hope, De Vrienden van UMC Utrecht and Mr M Spanbroek for their financial support. This work was supported by the Deep Learning for Medical Image Analysis research program by The Dutch Research Council P15-26 and Philips Research (SCW, MV and JPWP). Funders had no influence on study design, data collection or project management.

Competing interests

The authors declare no competing interests.

Additional information

Supplementary Information The online version contains supplementary material available at <https://doi.org/10.1038/s41598-022-19112-9>.

Correspondence and requests for materials should be addressed to M.V.

Reprints and permissions information is available at www.nature.com/reprints.

Publisher's note Springer Nature remains neutral with regard to jurisdictional claims in published maps and institutional affiliations.



Open Access This article is licensed under a Creative Commons Attribution 4.0 International License, which permits use, sharing, adaptation, distribution and reproduction in any medium or format, as long as you give appropriate credit to the original author(s) and the source, provide a link to the Creative Commons licence, and indicate if changes were made. The images or other third party material in this article are included in the article's Creative Commons licence, unless indicated otherwise in a credit line to the material. If material is not included in the article's Creative Commons licence and your intended use is not permitted by statutory regulation or exceeds the permitted use, you will need to obtain permission directly from the copyright holder. To view a copy of this licence, visit <http://creativecommons.org/licenses/by/4.0/>.

© The Author(s) 2022